

Supporting Information

Facile *In-situ* growth of Ni/Co-LDHs array by hypothermal chemical coprecipitation for all-solid-state asymmetric supercapacitors

By Tie Li^{*a}, Rui Li^b, and Hui Luo^a

a. *i*-Lab, Suzhou Institute of Nano-Tech and Nano-Bionics (SINANO), Chinese Academy of Sciences (CAS), 398 Ruoshui Road, Suzhou, 215123, P. R. China

b. College of Chemistry, Chemical Engineering and Materials Science, Soochow University, Jiangsu 215123, China.

*Email address: tli2014@sinano.ac.cn

Table of Contents

Fig. S1: The scheme for assembly structure and the actual photograph of the AAS.

Fig. S2: The sheet thickness distribution of the obtained Ni/Co-LDHs array.

Fig. S3: XRD patterns for Ni/Co-LDH arrays with different mole ratios.

Fig. S4: SEM images of Ni/Co-LDHs array obtained at reaction times.

Fig. S5: SEM images of the as-synthesized Ni/Co-LDHs array with various NaOH concentrations.

Fig. S6: SEM images of Ni/Co-LDHs array growth on fabric substrate at different Ni:Co ratios.

Fig. S7: SEM images of Ni/Co-LDHs array growth on CNT/rGO film at different Ni:Co ratios.

Fig. S8: SEM images of Ni/Co-LDHs array growth on Cu substrate at different Ni:Co ratios.

Fig. S9: (a) Comparison of CV and (b) GCD curves of the Ni/Co-LDHs array growth on Ni foam substrate; CV and GCD curves of the Ni/Co-LDHs array growth on various substrates: (c) and (d) Cu foil, (e) and (f) fabric, and (g) and (h) CNT/rGO film.

Fig. S10: Comparison of (a) GCD curves and (b) the specific capacitance of the Ni/Co-LDHs array growth on different substrates;

Fig. S11: (a) GCD curves of the pure Ni foam substrate; (b) CV and (b) GCD results and (d) the specific capacitance of the active carbon; (e) CV curves of the AFA-SCs device; (f) Comparison of Ragone plots of the AFA-SCs with references.

Table S1: Comparison of the maximum specific capacitance of some reported nickel-cobalt oxide/hydroxide based pseudocapacitive materials and this as-prepared electrode materials.

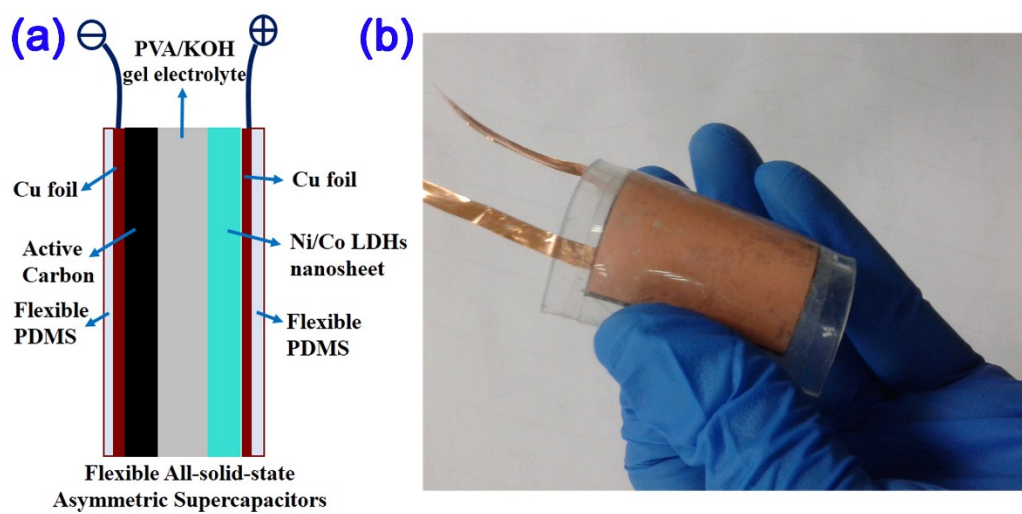


Fig. S1. (a) The scheme for assembly structure and (b) the actual photograph of the AAS based on the Ni/Co-LDHs nanosheet array growth on Cu foil and the active carbon.

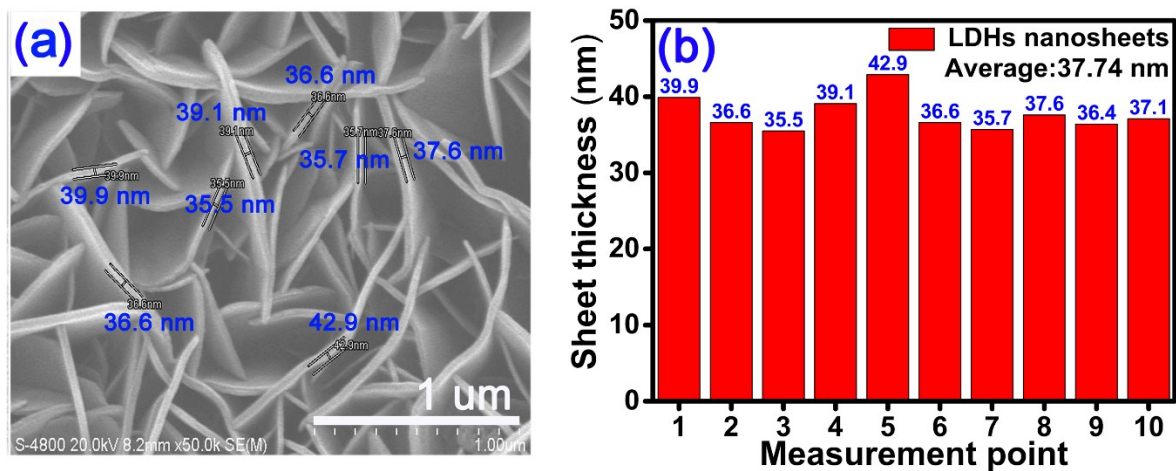


Fig. S2. (a) The dimension statistics and (b) the sheet thickness distribution of the obtained Ni/Co-LDHs array.

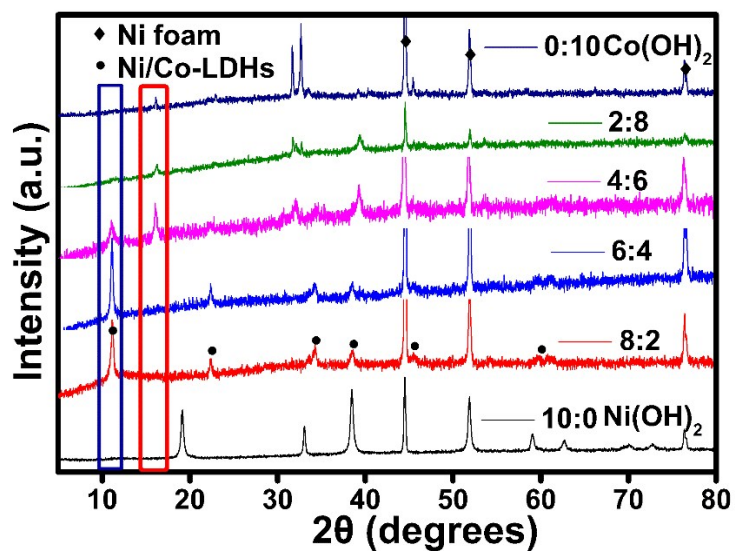


Fig. S3. The XRD patterns for Ni/Co-LDH arrays with different mole ratios: (a) 10:0, (b) 8:2, (c) 6:4, (d) 4:6, (e) 2:8, (f) 0:10.

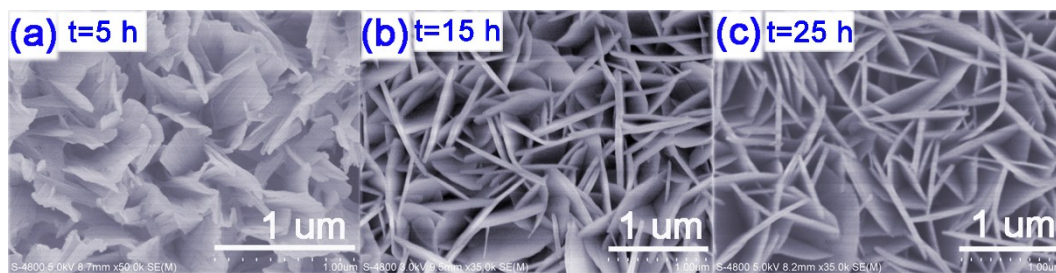


Fig. S4. SEM images of the Ni/Co-LDHs array obtained at various reaction times of (a) 1 h, (b) 15 h, and (c) 25 h.

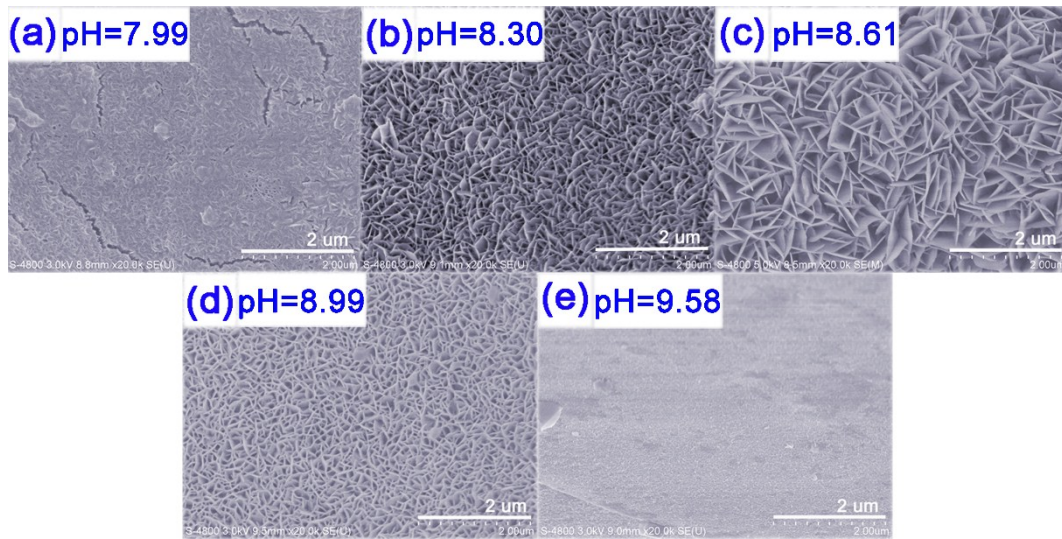


Fig. S5. SEM images of the as-synthesized Ni/Co-LDHs array obtained at 55 °C for 15 h with various NaOH concentrations: (a)1/4, (b) 1/2, (c) 1, (d) 1.5 and (e) 2.5 times of initial 1.375 mmol.

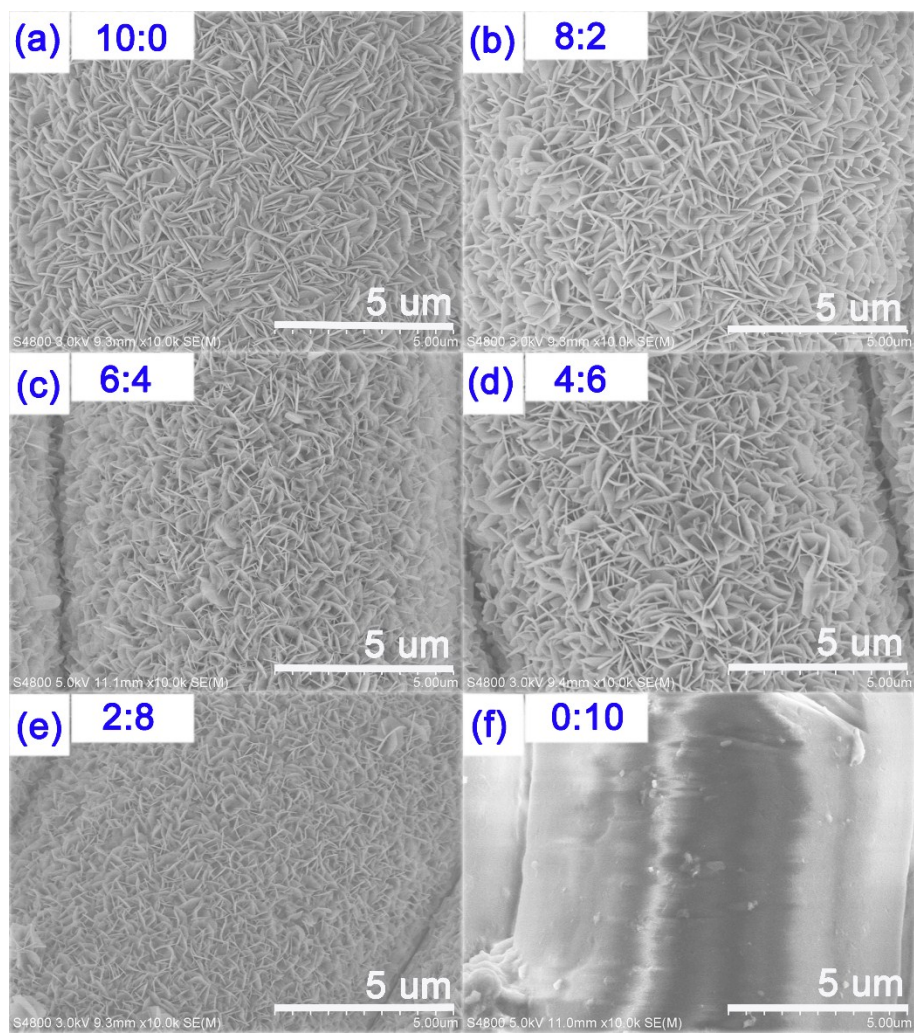


Fig. S6. SEM images of the Ni/Co-LDHs array growth on the fabric substrate obtained at different Ni:Co feeding mole ratios: (a) 10:0, (b) 8:2, (c) 6:4, (d) 4:6, (e) 2:8, (f) 0:10.

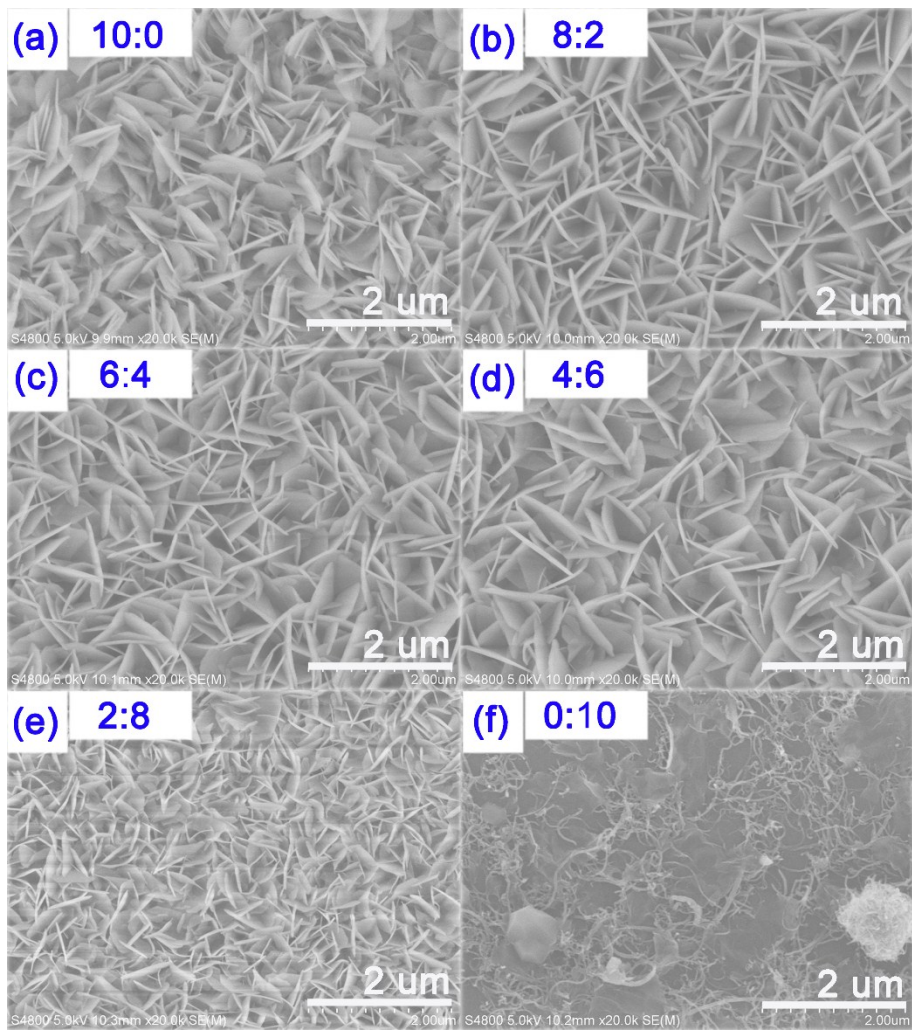


Fig. S7. SEM images of the Ni/Co-LDHs array growth on the CNT/rGO film substrate obtained at different Ni:Co feeding mole ratios: (a) 10:0, (b) 8:2, (c) 6:4, (d) 4:6, (e) 2:8, (f) 0:10.

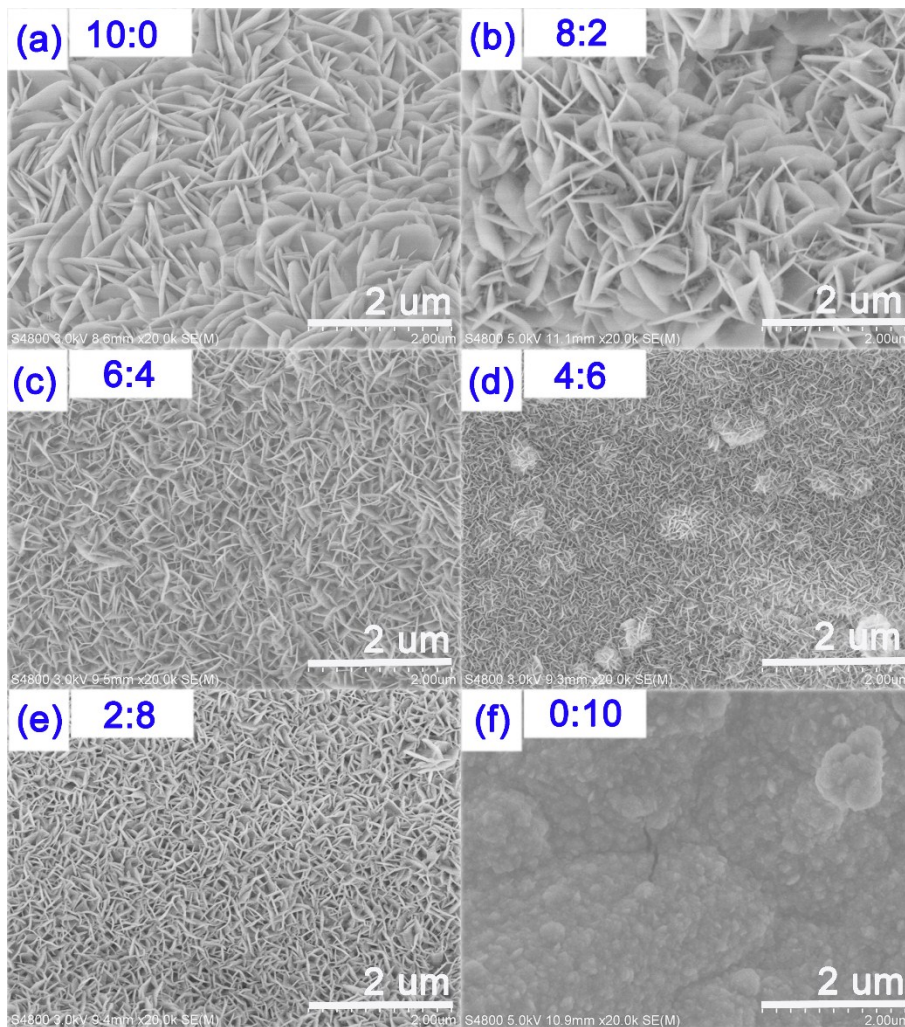


Fig. S8. SEM images of the Ni/Co-LDHs array growth on the Cu foil substrate obtained at different Ni:Co feeding mole ratios: (a) 10:0, (b) 8:2, (c) 6:4, (d) 4:6, (e) 2:8, (f) 0:10.

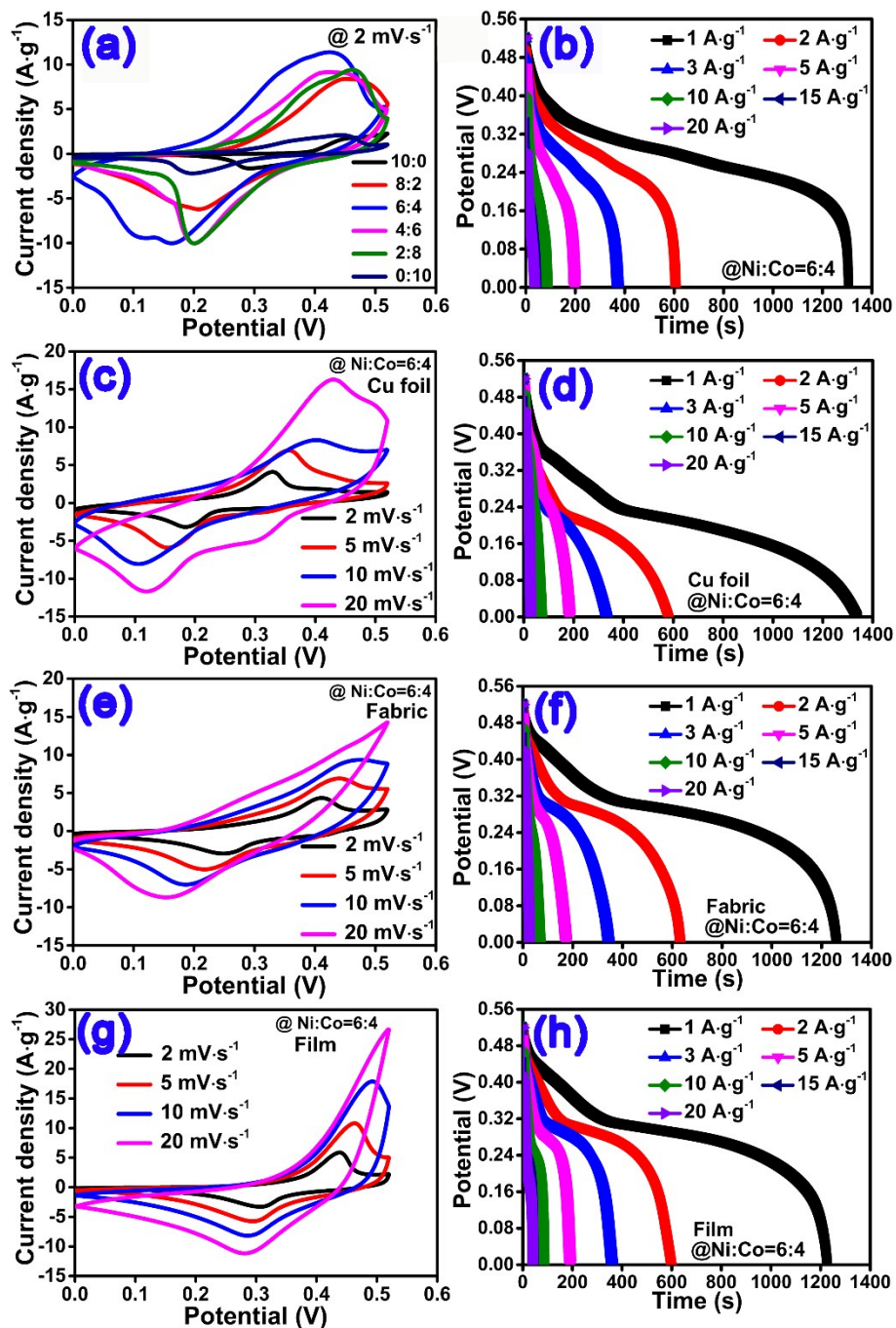


Fig. S9. (a) Comparison of CV curves of the Ni/Co-LDHs array growth on Ni foam substrate with different Ni:Co feeding mole ratios at a scan rate of $2 \text{ mV}\cdot\text{s}^{-1}$; GCD curves of (b) the Ni/Co-LDHs array growth on Ni foam substrate with $R=6:4$ at various current densities; CV and GCD curves of the Ni/Co-LDHs array growth on various substrates: (c) and (d) Cu foil, (e) and (f) fabric, and (g) and (h) CNT/rGO film.

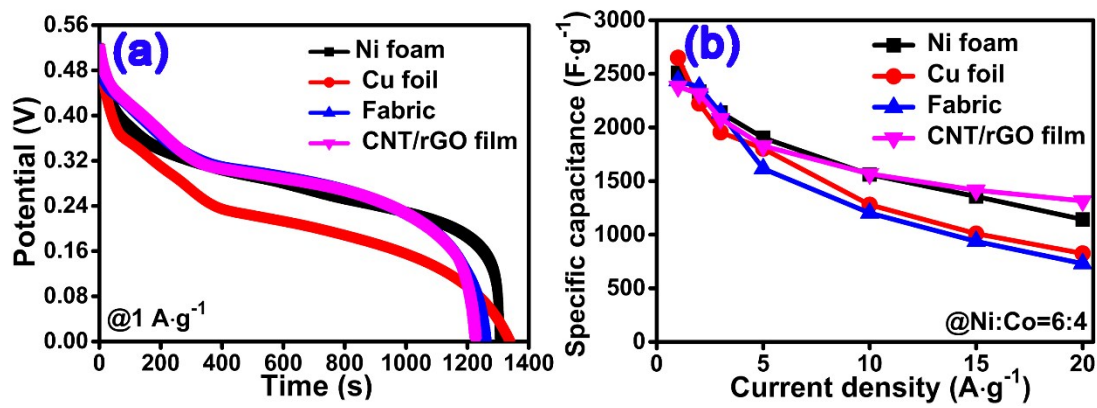


Fig. S10. Comparison of (a) GCD curves and (b) the specific capacitance of the Ni/Co-LDHs array growth on different substrates with Ni:Co ratio of 6:4 measured at $1 \text{ A}\cdot\text{g}^{-1}$.

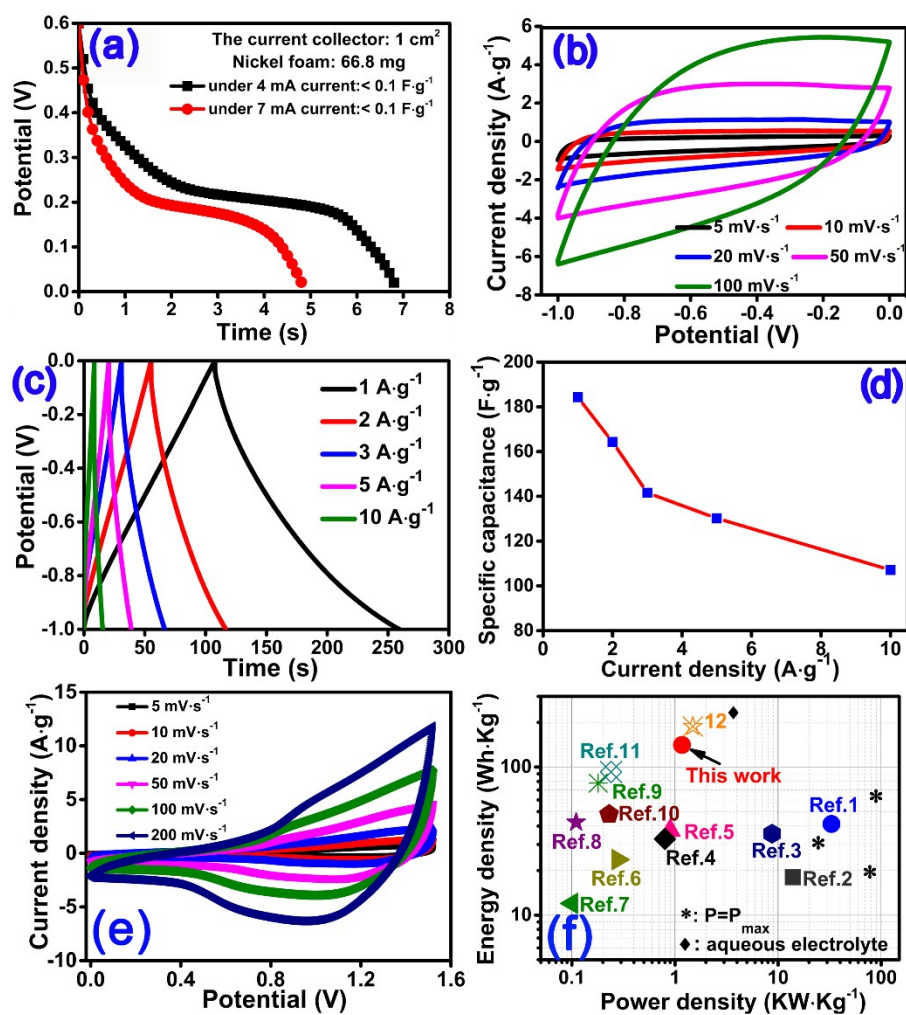


Fig. S11. (a) GCD curves of the pure Ni foam substrate; (b) CV and (b) GCD results and (d) the specific capacitance of the active carbon detected at various scan rates and current densities; (e) CV curves of the AFA-SCs device at scan rates of 5 mV·s⁻¹ to 100 mV·s⁻¹; (f) Comparison of Ragone plots of the AFA-SCs with references.

References:

- (1) L. Huang, D. C. Chen, Y. Ding, S. Feng, Z. L. Wang, and M. L. Liu, *Nano Lett.*, 2013, **13**, 3135.
- (2) Y. N. Meng, Y. Zhao, C. G. Hu, H. H. Cheng, Y. Hu, Z. P. Zhang, G. Q. Shi, and L. T. Qu, *Adv. Mater.*, 2013, **25**, 2326.
- (3) P. C. Chen, G. Z. Shen, Y. Shi, H. T. Chen, and C. W. Zhou, *ACS Nano*, 2010, **4**, 4403.

- (4) C. Tang, Z. Tang, and H. Gong, *J. Electrochem. Soc.*, 2012, **159**, 651.
- (5) U. M. Patil, S. C. Lee, J. S. Sohn, S. B. Kulkarni, K. V. Gurav, J. H. Kim, J. H. Kim, S. Lee, and S. C. Jun, *Electrochim. Acta*, 2014, **129**, 334.
- (6) X. Wang, A. Sumboja, M. Lin, J. Yan, and P. S. Lee, *Nanoscale*, 2012, **4**, 7266.
- (7) J. W. Zhao, J. L. Chen, S. M. Xu, M. F. Shao, Q. Zhang, Wei, F. J. Ma, M. Wei, D. G. Evans, and X. Duan, *Adv. Funct. Mater.*, 2014, **24**, 2938.
- (8) J. W. Lang, L. B. Kong, M. Liu, Y. C. Luo, and L. Kang, *J. Solid State Electrochem.*, 2010, **14**, 1533.
- (9) C. X. Yang, Y. L. Shi, N. S. Liu, J. Y. Tao, S. L. Wang, W. J. Liu, Y. M. Wang, J. Su, L. Y. Li, C. P. Yang, and Y. H. Gao, *RSC Adv.*; 2015, **5**, 45129.
- (10) H. Wang, Y. Y. Liang, T. Mirfakhrai, Z. Chen, H. S. Casalongue, and H. J. Dai, *Nano Res.*, 2011, **4**, 729.
- (11) L. B. Kong, M. Liu, J. W. Lang, Y. C. Luo, and L. Kang, *J. Electrochem. Soc.*, 2009, **156**, 1000.
- (12) H. Chen, L. F. Hu, M. Chen, Y. Yan, and L. M. Wu, *Adv. Funct. Mater.*, 2014, **24**, 934.

Table S1. Comparison of the maximum specific capacitance (C) based on active materials of some reported nickel-cobalt oxide/hydroxide based pseudocapacitive materials and this as-prepared electrode materials.

Active materials	Specific capacitance ($F \cdot g^{-1}$)	References
Ni-Co LDH/Ni foam	2682 ($3 A \cdot g^{-1}$)	(12) (high temperature and pressure/ surfactant)
Ni(OH) ₂ /Co(OH) ₂ composites	2193 ($2 A \cdot g^{-1}$)	(13)
Ni-Co oxide nanocomposites	287 ($0.2 A \cdot g^{-1}$)	(14)
NiCo ₂ O ₄ spinel	671 ($1 A \cdot g^{-1}$)	(15)
Co ₃ O ₄ /NiO nanowire arrays	853 ($2 A \cdot g^{-1}$)	(16)
Nickel-Cobalt Oxides (Sol-Gel)	1539 ($1 A \cdot g^{-1}$)	(17)
Ni-Co oxide/graphene oxide	1211.25 ($1 A \cdot g^{-1}$)	(18)
Ni-Co Hydroxide @Reduced Graphene Oxide	1691 ($0.5 A \cdot g^{-1}$)	(19)
Ni-Co Hydroxides on 3D Graphene Foam	1847 ($5 A \cdot g^{-1}$)	(20)
3D binary Ni-Co hydroxide/graphene	1410 ($2 A \cdot g^{-1}$)	(21)
Ni/Co-LDHs array	2510 ($1 A \cdot g^{-1}$)	This work

References:

- (12) H. Chen, L. F. Hu, M. Chen, Y. Yan, and L. M. Wu, *Adv. Funct. Mater.*, 2014, **24**, 934.
- (13) J. Li, M. Yang, J. Wei, and Z. Zhou, *Nanoscale*, 2012, **4**, 4498.
- (14) J. J. Deng, J. C. Deng, Z. L. Liu, H. R. Deng, and B. Liu, *J. Mater. Sci.*, 2009, **44**, 2828.
- (15) C. Wang, X. Zhang, D. Zhang, C. Yao, and Y. Ma, *Electrochim. Acta*, 2012, **63**, 220.
- (16) X. Xia, J. Tu, Y. Zhang, X. Wang, C. Gu, X. B. Zhao, and H. J. Fan, *ACS Nano*, 2012, **6**, 5531.
- (17) G. Hu, C. Tang, C. Li, H. Li, Y. Wang, and H. Gong, *J. Electrochem. Soc.*, 2011, **158**, 695.

- (18) Y. J. Xu, L. C. Wang, P. Q. Cao, C. L. Cai, Y. B. Fu, and X. H. Ma, *J. Power Sources*, 2016, **306**, 742.
- (19) H. N. Ma, J. He, D. B. Xiong, J. S. Wu, Q. Q. Li, V. Dravid, and Y. F. Zhao, *ACS Appl. Mater. Interfaces*, 2016, **8**, 1992.
- (20) U. M. Patil, J. S. Sohn, S. B. Kulkarni, S. C. Lee, H. G. Park, K. V. Gurav, J. H. Kim, and S. C. Jun, *ACS Appl. Mater. Interfaces*, 2014, **6**, 2450.
- (21) Y. Bai, W. Q. Wang, R. R. Wang, J. Sun, and L. Gao, *J. Mater. Chem. A*, 2015, **3**, 12530.